Utilization of image phase information to achieve super-sampling

JAMES N. CARON

Research Support Instruments, 4325-B Forbes Boulevard, Lanham, Maryland 20706, USA (Caron@RSImd.com)

For image phase-based super-sampling, an image sequence consisting of slightly displaced frames is up-sampled, aligned, and averaged into a single larger image that possesses image resolution exceeding the limitations of the imaging system. This process obtains a significant portion of high-resolution phase information and models the missing magnitude using deconvolution or reconstruction algorithms. Three simulations are presented in which a 32-frame sequence with the size 256 by 256 pixels is processed to create a single 4096 by 4096 pixel image with pixel level resolution. An empirical test was also conducted showing resolution beyond the digital sampling resolution limit of the camera. © 2020 Optical Society of America

1. INTRODUCTION

The resolution of a digital imaging system is limited by the optical cutoff as defined by the front aperture diameter and the digital sampling frequency limited by the pixel size on the focal plane array. Super-sampling, also referred to as super-resolution reconstruction (SRR), [1] is an image processing method that combines a sequence of slightly displaced images with the goal of producing a single larger image with resolution that exceeds the capability of the imaging system. The scene in the sequence is typically static, but the field of view (FOV) for each image is slightly shifted in order to provide sub-pixel information. While this method is generally used to improve resolution in video, [2–4] our interest is in the prospect of replacing a large monolithic telescope with an array of smaller, less expensive telescopes.

Most super-sampling methods consist of the following steps [5]:

1. Capture a sequence of images of a static scene where each frame is shifted providing sub-sampling information.
2. The pixel values of each image are aligned on a super-grid to create a single image.
3. A de-blurring method is applied to reveal increased image resolution.

In many techniques, alignment is achieved on a pixel-by-pixel basis. An algorithm is employed to determine the specific value for each pixel of the super-sampled image based on information from the frames, as with the Drizzle method [6]. Our approach [7], designated image phase alignment super-sampling (ImPASS), has the "instrument" images up-sampled, aligned, and averaged, as depicted in Fig. 1, producing a blurry image. Blind deconvolution, typically self-deconvolving data

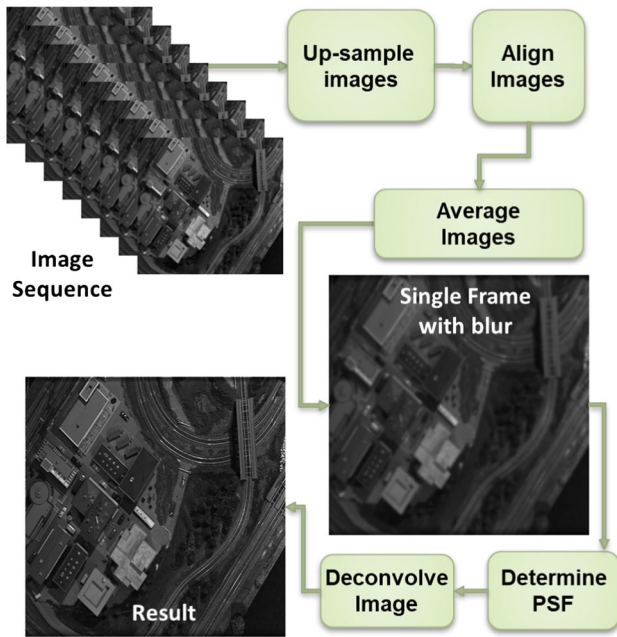restoration algorithm (SeDDaRA) [8], is applied to produce the high-resolution content.

Here, we discuss and demonstrate how ImPASS reveals scene features in the super-sampled image that are much smaller than a pixel in original instrument images. This is accomplished in frequency space by obtaining image phase information and modeling the missing magnitude information. This ability is demonstrated in three simulations and tested empirically. Application of ImPASS to simulated sets shows that with adequate knowledge of the translation differences between images and a good model for the spatial frequency distribution, high levels of image resolution can be achieved.

2. BACKGROUND

Image sequences used for super-sampling are typically produced by translating a camera while imaging a static scene [2,5], being first, to the best of our knowledge, described in 1984 [9] and applied on Voyager Martian images in 1993 [10]. The use of multiple cameras to capture the scene simultaneously, although fundamentally equivalent, has been reported more recently [11,12]. A camera/telescope array has the advantage of producing super-sampled images of dynamic scenes, but with increased cost and complexity.

While the benefits of super-sampling have been discussed at length in the literature [13], the limits of super-sampling are discussed less frequently. The figure of merit is magnification as defined by

$$M_{ss} \equiv \sqrt{\frac{\text{number of pixels in the super} - \text{sampled image}}{\text{number of pixels in instrument image}}},$$

(1)

Fig. 1. Flow chart for achieving a super-sampled image from a sequence of slightly displaced images of a static scene by applying image registration and blind deconvolution.

describing the upper limit of super-sampling that resolves objects with the size of a single pixel. Lin and Shum [14] first, to the best of our knowledge, described limitations based on the uncertainty in the registration method and noise. According to their paper, the level of magnification that can be achieved using reconstruction-based super-sampling is

$$M_{ss} < g(M_{ss})\sqrt{\frac{\hat{\delta}_h}{\delta_e + (\sigma_h + \hat{\delta}_h)\delta_p}}, \tag{2}$$

where $g(M_{ss})$ is a weighting function that has a maximum value of one, $\hat{\delta}_h$ is the average deviation of the signal, δ_e is the noise level, σ_h is the variation of details in the image (more variation provides more information to register the images), and δ_p is the accuracy of the image alignment. The authors used this formula to put an upper limit on M_{ss} of 1.6 in practical situations and 5.7 for synthetic situations. While the accuracy of the equation is debated in later articles [15,16], it reveals a common sense concept that the highest obtainable M_{ss} increases with increased signal-to-noise ratio (SNR) and decreases with uncertainty in image alignment. As such, one can achieve high M_{ss} if the relative positions of the low resolution and low noise images are precisely known. In later articles, Pham *et al.* discussed achieving $M_{ss} = 4$, and Robinson and Milanfar [15] suggested that $M_{ss} = 5$ can be obtained.

There has also been an increasing number of papers that describe achieving resolution from an optical system beyond the limit imposed by the front aperture diameter, such as works by Tsang *et al.* [17] and Wang *et al.* [18]. This is also expressed in a 2017 paper by Tham *et al.* [19].

For a given imaging system and a fixed number of collected photons, Tsang, Nair, and Lu observed that the Fisher information carried by the intensity of the light in the image plane

(the only information available to traditional techniques, including previous super-resolution approaches) falls to zero as the separation between the sources decreases; this is known as "Rayleigh's Curse." On the other hand, when they calculated the quantum Fisher information [20] of the full electromagnetic field (including amplitude and phase information), they found that it remains constant. In other words, there is infinitely more information available about the separation of the sources in the phase of the field than in the intensity alone.

While we are not claiming to achieve such a feat here, the concept that phase can be captured beyond limits of the imaging system is demonstrated with ImPASS [21,22].

3. MAGNITUDE AND PHASE

ImPASS succeeds by manipulating images in frequency space. The application of the Fourier transform to an image $I(x, y)$ produces a magnitude component and a phase component:

$$I(u, v) = \iint_{-\infty}^{\infty} I(x, y)e^{-2\pi i(xu+yv)}\,\mathrm{d}x\mathrm{d}y, \tag{3}$$

$$= |I(u, v)|e^{i\angle I(u,v)}, \tag{4}$$

where the magnitude $|I(u, v)|$ and phase $\angle I(u, v)$ can be calculated from the real and imaginary components produced by the transform using
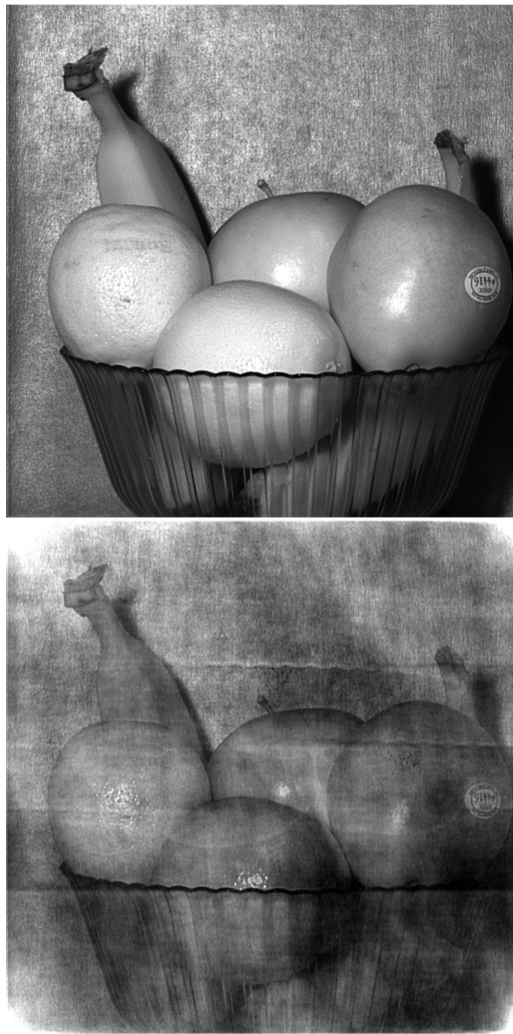
$$|I(u, v)| = \sqrt{I_r(u, v)^2 + I_i(u, v)^2}, \tag{5}$$

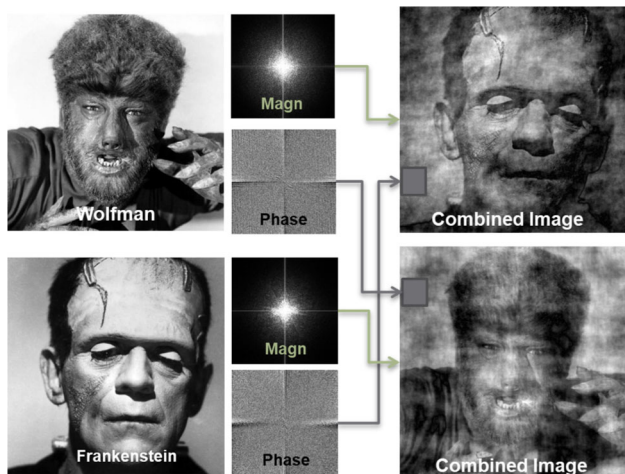$$\angle I(u, v) = \arctan[I_i(u, v)/I_r(u, v)], \tag{6}$$

where (u, v) are the coordinates in frequency space. Conceptually, the magnitude provides information about the distribution of spatial frequencies in an image. Low spatial frequencies are represented near the center and high frequencies near the borders. The phase provides information as to where the spatial frequencies are located and often resembles white noise. The phase defines points, edges, and shading in the image and produces the visual representation of the scene. If one alters the magnitude component in frequency space, application of an inverse Fourier transform produces a result that softens but does not remove features. However, when the phase is altered, as in Fig. 2, portions of the image disappear.

As an illustration, a fast Fourier transform (FFT) was applied to the images of Frankenstein and the Wolfman, shown in Fig. 3. The magnitude and phase components were swapped. An inverse FFT applied to each swapped image demonstrates that visual aspects of the scene follow the phase component. The hazy image artifacts are produced by the mismatch of the low frequency distributions in the two images. These artifacts are diminished if we retain the low spatial frequencies from each image, as demonstrated in Fig. 4. The final image is a combination of the whole phase from Frankenstein, the low frequency portion of the Frankenstein magnitude, and the high-frequency portion of the Wolfman magnitude.
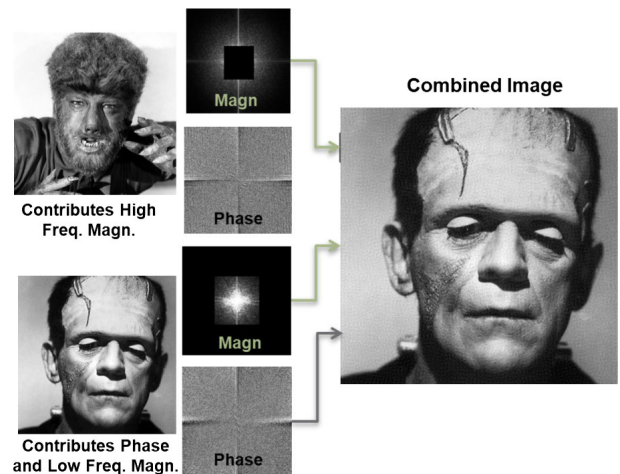
We have designated this process of replacing the magnitude of one image with another "Frankenstein" reconstruction, and it plays an important role in this analysis. When one applies a

Fig. 2. Phase of an image (top) was multiplied by 0.5 while in frequency space. The inverse transform (bottom) is missing elements and has artifacts.

Fig. 3. When the phase and magnitude of two images are swapped in frequency space, the image content follows the phase information. (Picture credits to Universal Studios, public domain.)

Fig. 4. If the low-frequency portion of the magnitude is preserved during the swap, artifacts from the Frankenstein reconstruction process are reduced.

deconvolution method to remove blur in an image, the deconvolution alters the magnitude to match a desired distribution but does not change the phase information. The Frankenstein technique explicitly replaces a portion of the magnitude with that from another image to achieve a desired distribution. A Frankenstein reconstruction can outperform a deconvolution method when a very good model of the scene is available, which is the case for our simulations. This allows us to improve the simulation and seek out limitations of the algorithm under optimum conditions.

4. PROCESSING APPROACH

Once an image sequence, $I_i(m, n)$, where i is in the frame index, has been captured or simulated, image registration is applied to measure the geometric differences between images. The differences can include rotation, scale, and perspective, but, for simplicity, our focus is restricted to translations. To measure the translational differences between images, phase correlation [23] is applied to the set of instrument images. If the alignments are known, such as the case with the simulations, this step can be bypassed. Each instrument image is up-sampled iteratively in scale steps of two using linear interpolation until the desired M_{ss} is reached. The images are aligned and averaged together. Deconvolution or reconstruction reshapes the magnitude to produce the final super-sampled image $I_{SS}(m, n)$.

We have employed four methods of deconvolution with varying levels of success: SeDDaRA, CARon, Frankenstein, and the interactive data language (IDL) version of maximum likelihood. SeDDaRA boosts the magnitude of a blurred image to match a non-blurred reference image with the desired distribution [8]. The CARon method is an approximation of SeDDaRA, where the reference image is replaced by a constant value [24]. Maximum likelihood is a common iterative deconvolution method with many variations [25].

When a single image of size 256 by 256 pixels (256^2 for brevity), for example, is up-sampled to 1024^2, there is no increase in spatial resolution. In Fourier space, the magnitude

of the up-sampled image has no additional information outside of the central 256^2 block. Even when additional up-sampled images are added together, no additional information outside of the 256^2 block is produced. As such, the higher resolution information produced by our process does not result from the combined magnitudes. Instead, the higher resolution is produced by the phase information from the combined images. Before reconstruction or deconvolution, the combined phase is being multiplied by empty space outside of the 256^2 block, or, as we have found, by artifacts associated with the interpolation process. Application of a deconvolution method, or Frankenstein, reforms that outer space towards a specific ideal such that multiplication of the combined phase elements by the new magnitude model produces an image with spatial resolution beyond the limits imposed by the camera system.

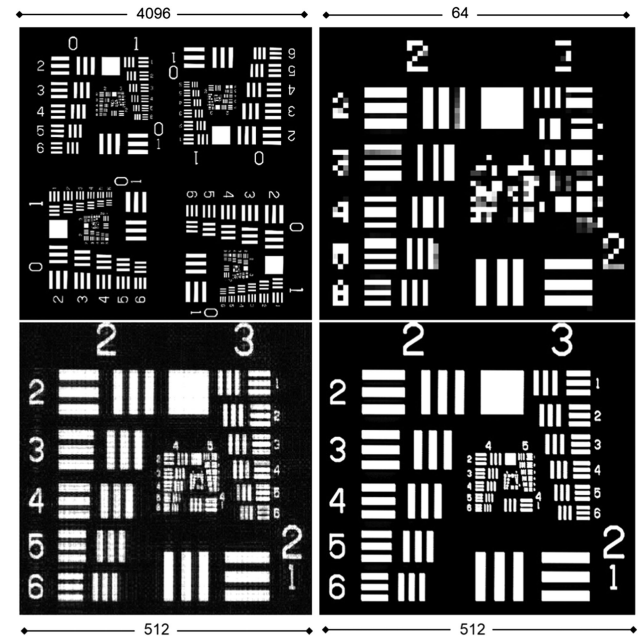## 5. SIMULATED IMAGE SETS AND PROCESSING RESULTS

The objective of the simulation is to create a sequence of smaller images with sub-pixel translations from a large image, representing the scene, for input to ImPASS. The process starts with the identification of the large image that serves as the control image, $I_c(m, n)$, having dimensions of $M_{ss}(M \times N)$ pixels, where $[M, N]$ are the dimensions of the instrument image. The following steps are applied:

1. A copy of the control image is created and designated as the target image, $I_t(m, n)$.
2. The target image is translated by a single pixel in either the X or Y direction. By limiting the motion to integer steps, artifacts introduced by interpolations are avoided.
3. If desired, blur can be added to the target image using convolution to better simulate an optical image.
4. Using multiple interpolation iterations, the target image is down-sampled to the M by N size, creating $I_i(m, n)$.
5. If desired, noise can be added to better simulate a digitally captured instrument image.
6. The process is repeated creating additional frames until there is sufficient sampling of the super-sampled pixel.

Multiple interpolations are required to ensure that all information in $I_t(m, n)$ is used to create a frame $I_i(m, n)$. With linear interpolation, for example, the value of a pixel is determined from neighboring pixels at the same location in the original image. If the change in scale is greater than 2, some original pixels are not used in the calculation of the interpolated pixel. That information is lost.

A. Air Force Chart

Our initial tests were performed on a 2048^2 sized United States Air Force (USAF)-style digital image. Initial tests using $M_{ss} = 4$ and $M_{ss} = 8$ proved successful. To study $M_{SS} = 16$, the USAF image was rotated in 90 deg increments and positioned to create a 4096^2 image, as shown in the Fig. 5 (top left). Using the simulation process, a sequence of 32 frames, with no noise or blur, was created and down-sampled to 256^2. A 64^2 portion of one frame of the instrument image set is shown in the top right to demonstrate the level of pixelation.

Fig. 5. Upper left corner is a 4096^2 image that was created from a 2048^2 digital representation of the USAF chart. A 64^2 region of the instrument image is shown in the top right. The restoration, in the lower left corner, possesses similar qualities to the truth image, lower right.

The frames were up-sampled to size 4096^2, aligned, and averaged together. The Frankenstein reconstruction is on the bottom left of Fig. 5, and a truth image is to the right. Close inspection shows that with full knowledge of the translations and a near-perfect model of the magnitude (an inverted truth image), we are able to recover the full resolution of the 4096^2 chart from a sequence of 256^2 images to achieve $M_{SS} = 16$.

An important question is how many frames are required in an image set to fully sample a super-sampled pixel. In an earlier test for $M_{SS} = 16$, our set consisted of 16 frames, where each frame was displaced by the equivalent of 1/16th of a pixel in both the $\hat{x}$ and $\hat{y}$ directions. The results were satisfactory, but the rounded portion of the numbers had a staircase quality. The frame count was increased to 32, where the first 16 frames were displaced by 1/16th of a pixel in the $\hat{x}$ direction, and the following 16 frames were displaced by 1/16th of a pixel in the $\hat{y}$ direction. With more images, the rounded portions of the numbers appear closer to the truth image in the processed result.

We also note that the processing produces some image artifacts that include ringing from edges and a cross-hatch pattern in flatter fields. These artifacts are created whether using either Frankenstein reconstruction or SeDDaRA deconvolution. Mitigation of the artifacts is left for further study.

B. Extended Scene

The method was then tested on an extended scene; an aerial image of Barcelona originally sized as 2048^2 and mirrored like the resolution chart to create a 4096^2 image. A sequence of thirty-two 256^2 frames with sub-pixels translation was created, where a 128^2 portion of the instrument image is shown in Fig. 6. Taking the magnitude model from the truth image,

Fig. 6.   (Top) The top-left quadrant, sized 128^2, of the instrument image from an extended scene. (Bottom) The top-left quadrant, sized 2048^2, in which the truth image was used to model the magnitude for the reconstruction. (Image used with permission, courtesy of Màrton Mogyorósy photography.)
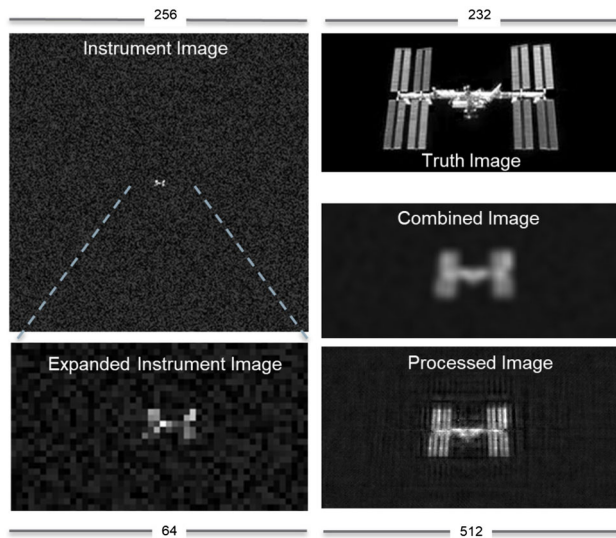

Fig. 7.   (Top) The same quadrant where a different aerial image was used for the magnitude model in the reconstruction. (Bottom) The quadrant where the 4096^2 USAF image was used as the magnitude model for the reconstruction.

the reconstruction exhibits vehicles and trees with significant detail that could only have been seen as individual pixels in the instrument image. The lines on the street and crosswalk in the middle, having a width of a pixel, are not at all visible in the instrument image. Aside from the 32-pixel border region, the level of resolution is consistent throughout the entire image.

By using the control image as the magnitude model, we are able to determine the effectiveness of the simulation process and assess the detail that is retained in the super-sampling process. In a real-world application, the truth image is not available. Figure 7 (top) shows a Frankenstein reconstruction that used an aerial image of New York for the magnitude model. Objects in the previous reconstruction are still apparent in this reconstruction. Pixel-sized street lines are still apparent. There is slightly

less sharpness to the edges, and the crosswalk in the middle is less clear. The reconstruction in Fig. 7 (bottom), using the USAF image from Fig. 5 for the magnitude model, shows additional image processing artifacts and reduced resolution primarily in the diagonal directions. Since the USAF image consists of mainly vertical and horizontal features, similar features in the reconstruction are still resolved.

C. Discrete Object with Noise

An image of the International Space Station (ISS), shown in Fig. 8 (top right), was pasted into a 4096^2 empty image. The simulation created thirty-two 256^2 slightly displaced frames
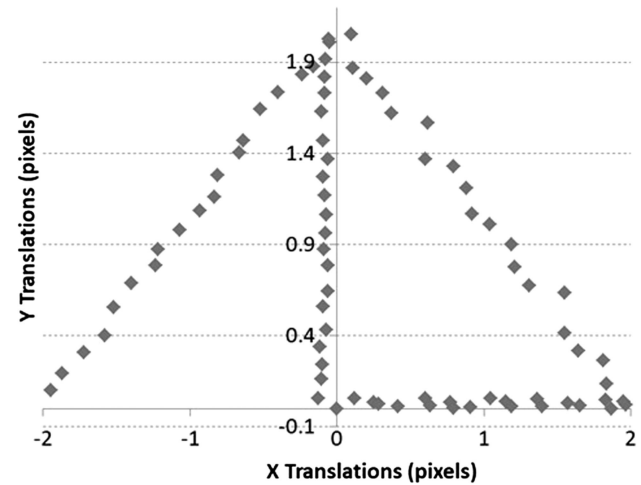
Fig. 8. Simulation and processing of an image of the ISS. The simulated set consisted of thirty-two 256^2 frames with added noise such that the SNR = 32. The top left shows the instrument image, which is expanded to on the bottom left to show the pixelation. After up-sampling and averaging, the image is blurry but does show detail well beyond the instrument image, as shown in the combined image. The process image has some processing artifacts, but the increased resolution is evident. (Image Credit: NASA.)

with additive noise such that SNR = 32. An expanded view of the instrument image reveals that the ISS only covers an 8×5 pixel region. The combined view shows the result of up-sampling, aligning, and averaging the images together. Even before processing, there is additional detail that cannot be resolved from the instrument image sequence. This information results from the multiplication of the new phase information by artifacts in the high-frequency area of the magnitude produced by the up-sampling interpolation method. The reconstruction shows some artifacts in the form of ringing. However, details of the ISS, including gaps between the solar panels and some features in the central hub are resolved. The noise in the final image was diminished by the averaging process, resulting in SNR = 142. When compared to a result that had no additive noise, the resolution was not significantly diminished.
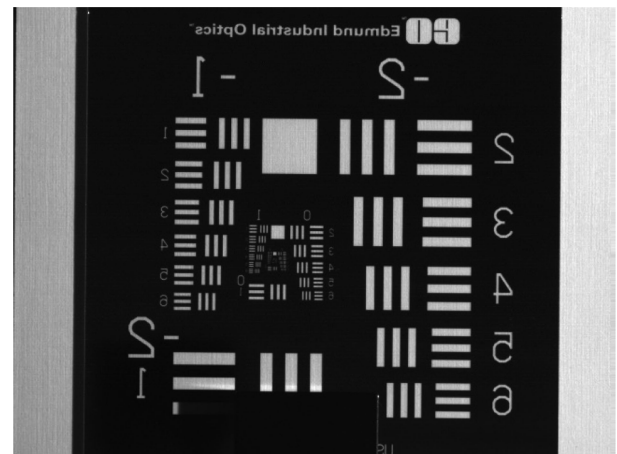
6. EMPIRICAL TEST AND RESULTS

To test ImPASS empirically, we positioned an Edmund Optics USAF target onto an $X - Y$ positioner. As the target was moved a single step in either the vertical or horizontal direction, an image was taken using a Sony XCD digital camera with 640 by 480 pixels. The camera lens has a focal length of 50 mm and a front aperture of 17.85 mm. Positioned about 1 m away from the target, the angular FOV for a 7.4 μm square pixel is 1.45 microradians. The Rayleigh cutoff for a wavelength of 630 nm is 0.43 microradians, limiting optical resolution on the sensor to 0.29 pixels. This arrangement mimics an array of cameras viewing a static scene from slightly different positions.

As mentioned above, ImPASS results are improved with improved knowledge of translations. The graph in Fig. 9 shows translations of the chart in pixels as measured using the phase
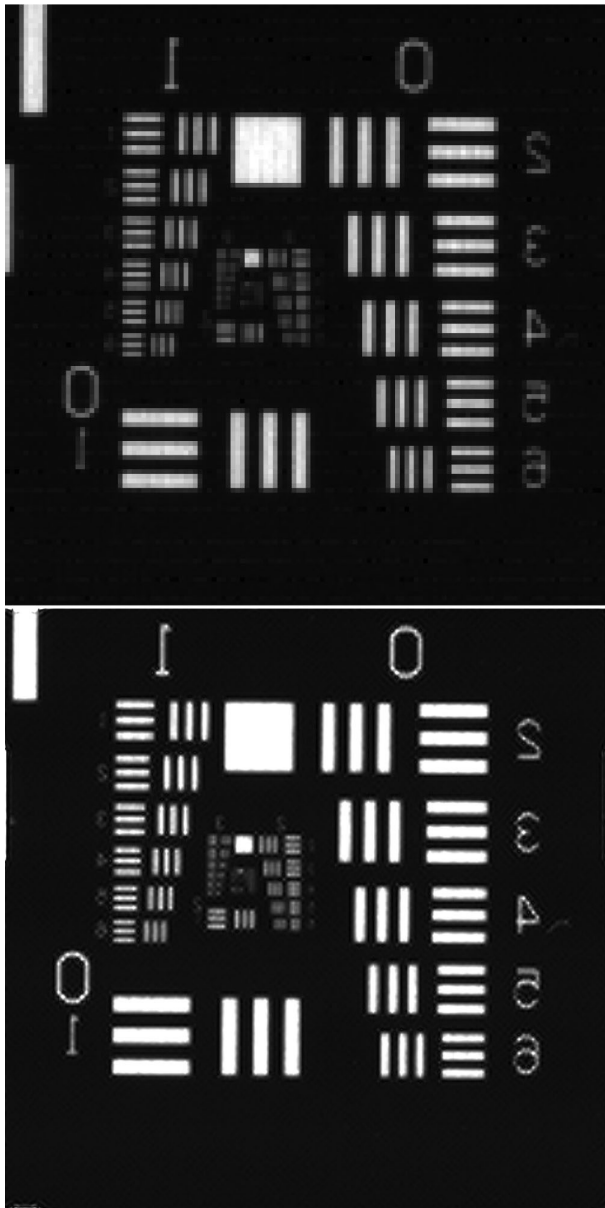

Fig. 9. Translation of the USAF chart by the stepper motor in terms of pixels as measured using image registration.

Fig. 10. Single 640×480 pixel frame of the USAF chart series.

correlation image registration [23]. Variations in the data are evident. With this setup, we cannot yet determine if variations are produced by uneven steps from the mechanical device or by errors in the image registration method.

The Edmund Optics USAF chart has a metallic mirror-like finish with the bars and numbers being transparent. The target was placed in the reverse (back-facing) position to avoid direct reflections from the illumination source. White card stock was positioned behind the transparent apertures to diffusely reflect light back to the camera. Eighty images were captured while moving the target in the "L + V" formation shown in Fig. 9. Each point on the graph is the measured distance in units of pixels between each frame of the sequence and the control frame (0,0). The objective is to produce enough sub-pixel information to produce a super-sampled image with the desired M_{ss}. A single frame, representing the instrument image, is shown in Fig. 10 and has a SNR = 98. The images were up-sampled to size to 5120×3840 (potentially $M_{ss} = 8$) and aligned using the measured translations times eight. The up-sampled aligned images were averaged into a single image, which was then cropped to 1024^2 to ease processing.

Fig. 11. (Left) The central portion (128^2 pixels) of an instrument image. (Right) The central 512^2 area after application of ImPASS. Additional resolution can be seen, but not to the level of the simulations.

A 128^2 portion of the instrument image is shown in Fig. 11, showing pixelation of the bars and numbers. The processed version, using the SeDDaRA approximation [24], shows increased resolution that has some image artifacts. Many features in the processed image cannot be seen in the instrument image, such as the numbers 1 to 6 running down the left side. The shape of the numbers 2 and 3 can be discerned, and the bars are resolved down to the 2–3 series, as opposed to the 1–2 series in the instrument image. According to military standard (MIL-STD) 150 A, this is an improvement in resolution from 0.223 mm to 0.099 mm, which is a 2.25 improvement in the resolution. It is evident that we have produced resolution beyond the sampling spatial frequencies of the camera. The hope was to show resolution beyond the Rayleigh cutoff as Tsang theorized [17],

but success may have been limited by the setup. Potential issues could be the uncertainties in the alignment, a mismatch between the deconvolution, and the type of point spread function, noise, or a combination of these factors.

7. CONCLUSION

This paper describes the concept, process, and application of ImPASS. The ability of the approach to produce image resolution beyond the capabilities of the camera system stems from obtaining phase information beyond the original image size and modeling the missing magnitude using deconvolution or Frankenstein reconstruction. The method was applied successfully, achieving $M_{ss} = 16$ for a digital USAF chart, an extended scene, and a small object with noise. Different magnitude models were used for the extended scene, showing only slight variations in resolution. Resolution was consistent across the extended scene aside from a border of 32 pixels. Important considerations for successful application of ImPASS include good knowledge of the displacements, acquired from a predetermined set-up or an image alignment algorithm, and sufficiently sampling the super-sampled pixel. While a full investigation of noise was beyond the scope of the study, we demonstrated that as a result of averaging, the final result can have higher SNR than an instrument image, even after reconstruction.

The application of this algorithm to an empirical image set was successful in obtaining information beyond the digital sampling limit of the camera. The level of improvement was considerably less than that achieved in the simulations. Further study is warranted to determine whether the results are limited by the uncertainties in the setup, insufficient sampling of the scene, or the optical resolution of the imaging system.

Disclosures. The author declares no conflicts of interest.

REFERENCES

1. R. Driggers, K. Krapels, and S. Young, "The meaning of super-resolution," Proc. SPIE **5784**, 103–106 (2005).
2. J. M. Schuler and D. A. Scribner, "Increasing spatial resolution through temporal super-sampling of digital video," Opt. Eng. **38**, 801–806 (1999).
3. M. K. Ng, H. Shen, E. Y. Lam, and L. Zhang, "A total variation regularization based super-resolution reconstruction algorithm for digital video," EURASIP J. Adv. Signal Process. **2007**, 1–16 (2007).
4. M. Moustafa, H. M. Ebied, A. Helmy, T. M. Nazamy, and M. F. Tolba, "Optimization methods for medical image super resolution reconstruction," in *Applications of Intelligent Optimization in Biology and Medicine* (Springer, 2016), pp. 135–157.
5. V. Patanavijit, "Super-resolution reconstruction and its future research direction," AU J. Technol. **12**, 149–163 (2009).
6. A. S. Fruchter and R. N. Hook, "Drizzle: a method for the linear reconstruction of undersampled images," Publ. Astron. Soc. Pac. **114**, 144–152 (2002).
7. J. N. Caron, "Rapid supersampling of multiframe sequences by use of blind deconvolution," Opt. Lett. **29**, 1986–1988 (2004).

8. J. N. Caron, N. M. Namazi, and C. J. Rollins, "Noniterative blind data restoration by use of an extracted filter function," Appl. Opt. **41**, 6884–6889 (2002).

9. T. S. Huang, "Multi-frame image restoration and registration," Comput. Vis. Image Process. **1**, 317–339 (1984).

10. P. Cheeseman, B. Kanefsky, R. Kraft, J. Stutz, and R. Hanson, "Super-resolved surface reconstruction from multiple images," in *Maximum Entropy and Bayesian Methods* (Springer, 1996), pp. 293–308.

11. G. Carles, J. Downing, and A. R. Harvey, "Super-resolution imaging using a camera array," Opt. Lett. **39**, 1889–1892 (2014).

12. J. Fan, X. Zeng, Q. Huangpeng, J. Zhou, and J. Feng, "A depth-based super-resolution method for multi-view color images," Proc. SPIE **10011**, 100110N (2016).

13. K. Nasrollahi and T. B. Moeslund, "Super-resolution: a comprehensive survey," Mach. Vis. Appl. **25**, 1423–1468 (2014).

14. Z. Lin and H.-Y. Shum, "Fundamental limits of reconstruction-based superresolution algorithms under local translation," IEEE Trans. Pattern Anal. Mach. Intell. **26**, 1073–1078 (2004).

15. D. Robinson and P. Milanfar, "Statistical performance analysis of super-resolution," IEEE Trans. Image Process. **15**, 1413–1428 (2006).

16. T. Q. Pham, L. J. van Vliet, and K. Schutte, "Influence of signal-to-noise ratio and point spread function on limits of superresolution," Proc. SPIE **5672**, 169–180 (2005).

17. M. Tsang, R. Nair, and X.-M. Lu, "Quantum theory of superresolution for two incoherent optical point sources," Phys. Rev. X **6**, 031033 (2016).

18. C. Wang, D. Tang, Y. Wang, Z. Zhao, J. Wang, M. Pu, Y. Zhang, W. Yan, P. Gao, and X. Luo, "Super-resolution optical telescopes with local light diffraction shrinkage," Sci. Rep. **5**, 18485 (2015).

19. W.-K. Tham, H. Ferretti, and A. M. Steinberg, "Beating Rayleigh's curse by imaging using phase information," Phys. Rev. Lett. **118**, 070801 (2017).

20. D. Petz and C. Ghinea, "Introduction to quantum Fisher information," Quantum Probab. Relat. Top. **1**, 261–281 (2011).

21. M. Dewitt, Senior Program Manager, Intelligence Advanced Research Projects Activity, College Park, Maryland, USA (personal communication, 2019).

22. J. Altepeter, Program Manager, Defense Advanced Research Projects Agency, Arlington, Virginia, USA (personal communication, 2020).

23. J. N. Caron, M. J. Montes, and J. L. Obermark, "Extracting flat-field images from scene-based image sequences using phase correlation," Rev. Sci. Instrum. **87**, 063710 (2016).

24. J. N. Caron, N. M. Namazi, R. L. Lucke, C. J. Rollins, and P. R. Lynn, "Blind data restoration with an extracted filter function," Opt. Lett. **26**, 1164–1166 (2001).

25. F. Varosi and W. B. Landsman, "An IDL based image deconvolution software package," in *Astronomical Data Analysis Software and Systems II* (1993), Vol. **52**, p. 515.